Journal of Alloys and Compounds 509 (2011) 6067–6071

Contents lists available at ScienceDirect

Journal of Alloys and Compounds

journal homepage: www.elsevier.com/locate/jallcom

Theoretical study on the electronic and optical properties of (N, Fe)-codoped anatase TiO_2 photocatalyst

Lichao Jia[a], Congcong Wu[a], Song Han[b], Nian Yao[a], Yuanyuan Li[a], Zongbao Li[c], Bo Chi[a,*], Jian Pu[a], Li Jian[a]

[a] School of Materials Science and Engineering, State Key Lab of Material Processing and Die & Mould Technology, Huazhong University of Science and Technology, Wuhan, Hubei 430074, China
[b] College of Forestry, Northeast Forestry University, Harbin 150040, China
[c] Department of Physics, Tongren University, Guizhou 554300, China

ARTICLE INFO

Article history:
Received 7 December 2010
Received in revised form 1 March 2011
Accepted 2 March 2011
Available online 10 March 2011

Keywords:
Anatase TiO_2
Doping
Visible-light photocatalyst
First-principle

ABSTRACT

Electronic and optical properties of pure, N-doped, Fe-doped and (N, Fe)-codoped anatase TiO_2 were evaluated, respectively, by using the density functional theory. The results indicate that the elemental doping narrows the band gap of TiO_2 and realize its visible-light response activity; and incorporation of Fe into N-doped TiO_2 further increases the photocatalytic activity under visible-light irradiation compared with that of the N-doped TiO_2.

1. Introduction

Titania has been widely studied as a promising material for photochemical applications due to its excellent properties, such as chemical stability, non-toxicity, low cost, etc. [1–4] However, anatase TiO_2 shows photocatalytic activity only under ultraviolet light irradiation ($\lambda < 385$ nm) because of its wide band gap (~3.20 eV), which leads to a low solar energy utilization with pure anatase TiO_2 [5]. Great efforts have been made to modify the electronic property of TiO_2 in order to extend its optical absorption edge into visible-light region and enhance its visible-light photocatalytic activity. An effective approach is doping the TiO_2 with metal or non-metal elements [6–10].

Since Sato reported for the first time that N-doped TiO_2 showed visible-light photocatalytic activity [11], many studies have been conducted to investigate the doping effect of TiO_2 theoretically and experimentally [12–17]. Most of these studies concentrated on mono-doping of the TiO_2 with metal or non-metal ions. Doping by non-metal ions can extend the optical absorption edge [18] of the TiO_2 by means of narrowing its band gap; however, the narrowed band gap results in an increased recombination rate of photo-excited carriers, reducing the photo-excited current or photocatalytic efficiency [19,20]. And the transition metal doping promotes the photocatalytic efficiency, with the existence of carrier recombination centers and strongly localized d states in the band gap, which reduces the carrier mobility significantly [21]. Recent studies suggested that introducing metal ions into nonmetal doped TiO_2 can make the metal ions as a mediator for interfacial charge transfer, and prevent the recombination of electron–hole pairs. Therefore, the synergistic effect of codoping with nonmetal and metal ions into the TiO_2 can extend the absorption edge into visible-light range and noticeably promote the efficiency of photocatalysis [22–27].

It has been reported recently that adding Fe to N-doped TiO_2 significantly increases the photocatalytic activity under visible-light irradiation [28]. The doping of N into TiO_2 can enhance the photo-response in visible-light region and that of Fe can reduce the recombination of electrons and holes. Both of these two effects are beneficial to the improving the performance of (Fe, N)-codoped TiO_2 photocatalyst. However, the mechanism of such enhancement has not been studied in detail. In the present work, the electronic and absorption properties of (N, Fe)-codoped TiO_2 have been investigated by using the density functional theory (DFT) to reveal the microscopic mechanism for band gap narrowing and the origin of the enhanced photocatalytic activity. For comparison, the corresponding calculation and theoretic

* Corresponding author. Tel.: +86 27 87558142; fax: +86 27 87558142.
E-mail address: chibo@hust.edu.cn (B. Chi).

0925-8388/$ – see front matter © 2011 Elsevier B.V. All rights reserved.
doi:10.1016/j.jallcom.2011.03.012

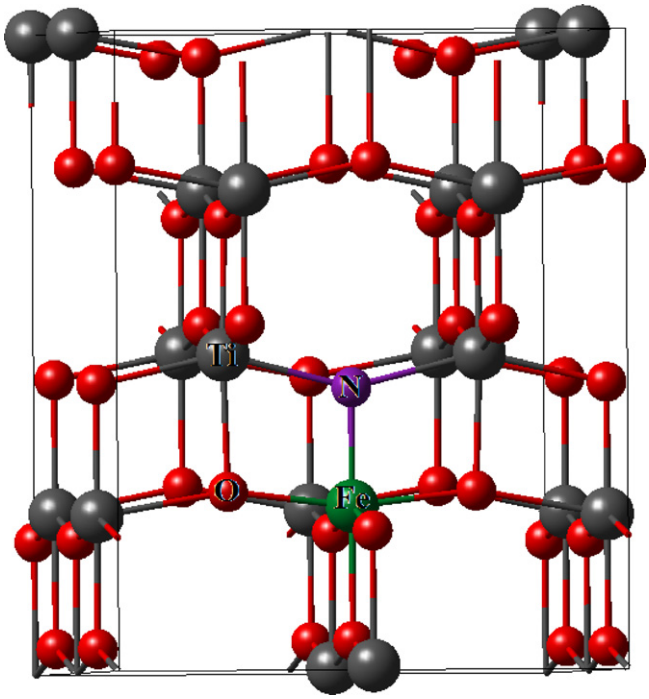

Fig. 1. Supercell model for defective anatase TiO_2 showing the location of the dopants. The ion doping sites are marked with N and Fe. The large grey spheres and the small red spheres represent Ti and O atoms, respectively. (For interpretation of the references to color in this figure legend, the reader is referred to the web version of the article.)

analysis were also conducted for pure, N-doped and Fe-doped anatase.

2. Calculation details

The unit cell of anatase TiO_2 (Ti_4O_8) has a symmetry of space group $D_{4h}^{19} - I_{41}/amd$. The doped systems were constructed from a relaxed $(2 \times 2 \times 1)$ 48-atom anatase supercell, as shown in Fig. 1. In N- or Fe-doped TiO_2 model, an O atom is substituted by an N atom or a Ti atom is substituted by an Fe atom. (N, Fe)-codoped TiO_2 is modeled by single substitution of an N atom for an O atom, and one of its adjacent Ti atoms is replaced by an Fe atom in the supercell. Although it is assumed that there are no oxygen vacancies in the doped systems, neglecting the effects of oxygen vacancies on the properties of the (N, Fe)-codoped anatase TiO_2 in calculations, the oxygen vacancies may be formed in the structure caused by doping in practice, due to the requirement of charge balance. Iijima et al. [29] studied the influence of oxygen vacancies on optical properties of anatase TiO_2 thin films, and it was found that the oxygen vacancy states were widely distributed in the region below 2.5 eV, in which a broad absorption peak was observed.

All the spin-polarized calculations were performed using the projector augmented wave (PAW) pseudopotentials as implemented in the Vienna ab-initio simulation package (VASP) [30,31]. The exchange correlation function was treated within the Generalized Gradient Approximation (GGA) and parameterized by Perdew–Burke–Ernzerhofer (PBE) formula [32]. The Brillouin-zone integrations were approximated by using the special k-point sampling of the Monhkorst-Pack scheme [33]. A cutoff energy of 400 eV and a mesh size of $4 \times 4 \times 4$ were used for geometry optimization and electronic property calculations. Using the block Davidson scheme, both the atomic positions and cell parameters were optimized until the residual force was below 0.01 eV/Å. It is well known that the GGA method underestimates the band gap of the TiO_2 significantly in comparison with the experimental result (2.0 eV vs. 3.2 eV). In order to obtain the band gap that is consistent with the experimental result, the so-called GGA + U method [34] was employed to amend the difference. The Coulombic interaction U and exchange energy J were set to be 6.3 eV and 1 eV, respectively. Accordingly, the calculated band gap of pure anatase TiO_2 was 3.08 eV, which is in good agreement with the experimental value of 3.20 eV [35].

Table 1
Average bond lengths of the doped TiO_2 after geometry optimization.

Bond length (Å)	Pure TiO_2	N-doped	Fe-doped	Codoped
Ti–O	1.976	1.980	1.978	1.962
Ti–N		2.008		2.001
Fe–O			1.915	1.889
Fe–N				1.776

For optical properties the complex dielectric function $\varepsilon = \varepsilon_1 + i\varepsilon_2$, the imaginary part ($\varepsilon_2$) and the real part ($\varepsilon_1$)were calculated theoretically based on the DFT. The corresponding absorption spectrum was estimated using the following equation:

$$I(\omega) = 2\omega \left(\frac{\left[\varepsilon_1^2(\omega) + \varepsilon_2^2(\omega)\right]^{1/2} - \varepsilon_1(\omega)}{2} \right)^{1/2}$$

The valence electron configurations considered in this study included Ti ($3d^2 4s^2$), O ($2s^2 2p^4$),N ($2s^2 2p^3$) and Fe ($3d^6 4s^2$).

3. Result and discussion

3.1. Geometry analysis

After structure optimization of the pure anatase TiO_2 supercell, the lattice parameters were obtained as follows: $a = b = 3.8176$ Å, $c = 9.4801$ Å. These data are in good agreement with the measured results [36], which implies that the calculation methods are reasonable and the calculated results are considered to be reliable.

The average bond lengths of the doped TiO_2 after geometry optimization are summarized in Table 1. For pure TiO_2, the average Ti–O bond length is 1.976 Å; there is no significant change compared with that of the N or Fe doped one. However, the average Ti–O bond length in the supercell is shorter in the N and Fe codoped TiO_2. The average Ti–N bond length in N-doped and (N, Fe)-codoped systems are longer than the Ti–O bond length as the radius of N ion is slightly larger than that of O ion. Due to the smaller radius of Fe, the average Fe–O bond length of Fe-doped and the codoped TiO_2 is shorter than that of the Ti–O bond. In the case of codoped TiO_2, the length of all these bonds is decreased. The results indicate that N and Fe codoping leads to an obvious lattice distortion, which in turn changes the dipole and moments, makes the separation of photo-excited electron–hole pairs easier.

3.2. Electronic structure

The band structure of the four various TiO_2 based materials was obtained by the GGA + U calculations, as shown in Fig. 2. The Fermi level is set to 0 eV on the energy axis; the red lines refer to the up-spin states, while the blue ones refer to the down-spin states. It can be seen from Fig. 2a, the calculated band gap of pure anatase TiO_2 is 3.08 eV, which is consistent with previous experimental and calculation results [27,35]. Only red lines can be observed because of the overlap of the up-spin and down-spin states. And the valence band and conduction band moves to low energy states with doping. The calculated band gap of the N-doped, Fe-doped and (N, Fe)-codoped TiO_2 is 2.77, 2.76 and 2.73 eV, respectively, regardless of the impure states. In the case of the N-doped TiO_2 (Fig. 2b), an impure state is

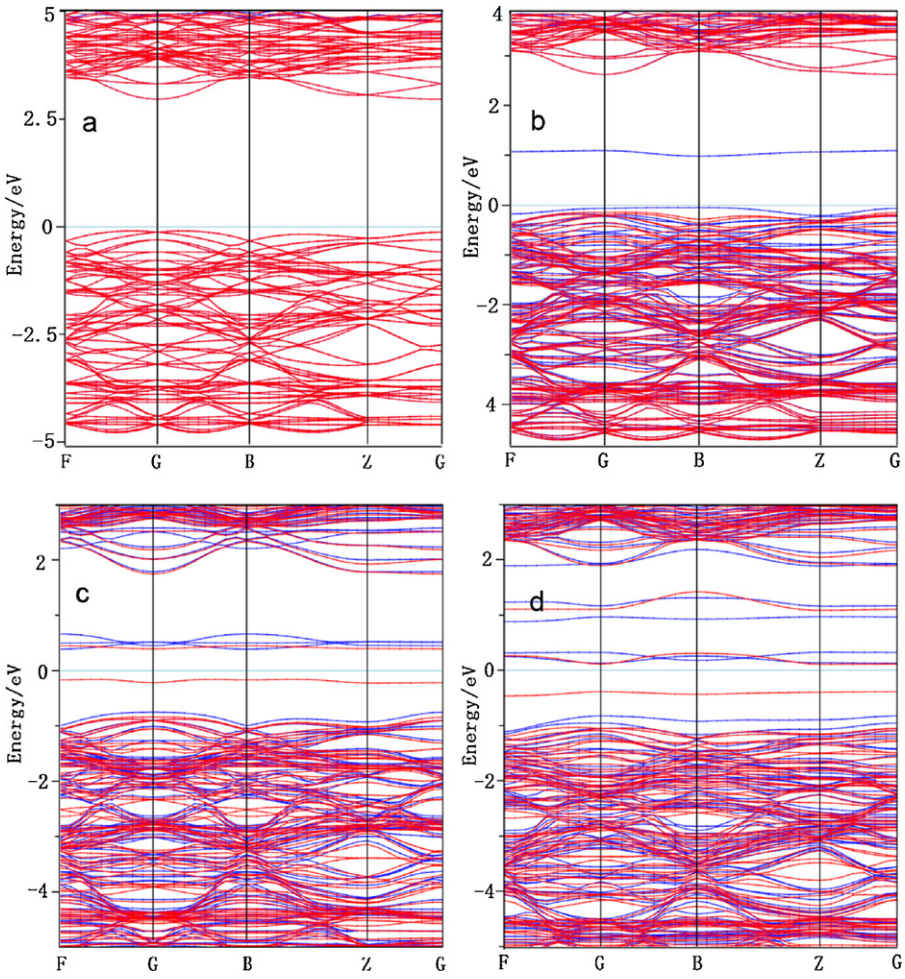

Fig. 2. Calculated band structure of: (a) pure TiO_2, (b) N-doped TiO_2, (c) Fe-doped TiO_2 and (d) (N, Fe)-codoped TiO_2. The Fermi level is set to be 0 eV on the energy axis. The red lines refer to the up-spin states and the blue ones refer to the down-spin states.

located above the valence band maximum (VBM) that can accept electrons from the valence band and then transfer them to the conduction band, which may cause significant red-shift in the fundamental absorption edge of anatase TiO_2. In the Fe-doped TiO_2 (Fig. 2c), two kinds of impure states are located in the band gap: one is above the VBM and the other is below the conduction band minimum (CBM). And in the case of the codoped TiO_2 (Fig. 2d), several impure states appear in the forbidden gap. With the decrease of the symmetry of crystal structure caused by elemental doping, the impure energy levels split obviously into the band gap above the VBM and below the CBM. It is the existence of these impure energy levels in the band gap that reduces the carrier transition energy and makes it possible for electrons in the valence band to be excited step by step to the conduction band, beneficial to the separation of photo-excited electron–hole pairs. As a consequence, the sensitive light wavelength of the codoped anatase TiO_2 is extended into the region of visible-light, promoting the adsorption of visible light.

To further understand the origin of the band-gap variation with N and/or Fe (co)doping, the density of states (DOS) and projected density of states (PDOS) were calculated and plotted in Fig. 3 for all the undoped and doped anatase, with up-spin DOS above zero and down-spin DOS below zero. In the pure anatase TiO_2 (Fig. 3a), the valence band is dominated by O 2p state, while the conduction band by Ti 3d state. In the N-doped anatase TiO_2 (Fig. 3b), N 2p state are split into two parts, i.e. above and below the Fermi level. The impure energy levels below the Fermi level sufficiently overlap with the VBM of anatase TiO_2. In the Fe-doped TiO_2 (Fig. 3c), the new energy levels are formed because of the hybridization effect between Fe 3d state and Ti 3d state. In (N, Fe)-codoped TiO_2 (Fig. 3d), the hybridized states arise from N 2p and Fe 3d orbits with minor contribution of O 2p, whereas the CBM is composed primarily of empty Fe 3d and Ti 3d orbits. The hybridization effects can promote the migration of photo-excited carriers and the process of photocatalysis. These impure states above the Fermi level may trap the photo-excited electrons, while those below Fermi level may trap the photo-excited vacancies, improving the transfer of the photo-excited carriers to the reactive sites.

3.3. Optical properties

Based on the obtained electronic structures, the optical absorption spectra of the pure and doped TiO_2 were calculated, and anisotropic spectra, as shown in Fig. 4, were obtained due to the crystal structure of TiO_2. Thus the absorption coefficient should be analyzed in several directions. In the present study, the absorption spectra along the *X* axis were chosen to analyze the effect of the doping. From Fig. 4, it is found that pure anatase TiO_2 can only respond to the UV light and shows no absorption activity to the visible-light, while the introduction of impure atoms into the TiO_2 results in a noticeable red-shift effect. Generally, elemental doping promotes the shift of the fundamental absorption edges towards the visible-light region. This phenomenon is more obvious in (N, Fe)-codoped TiO_2 than N-doped and Fe-doped TiO_2.

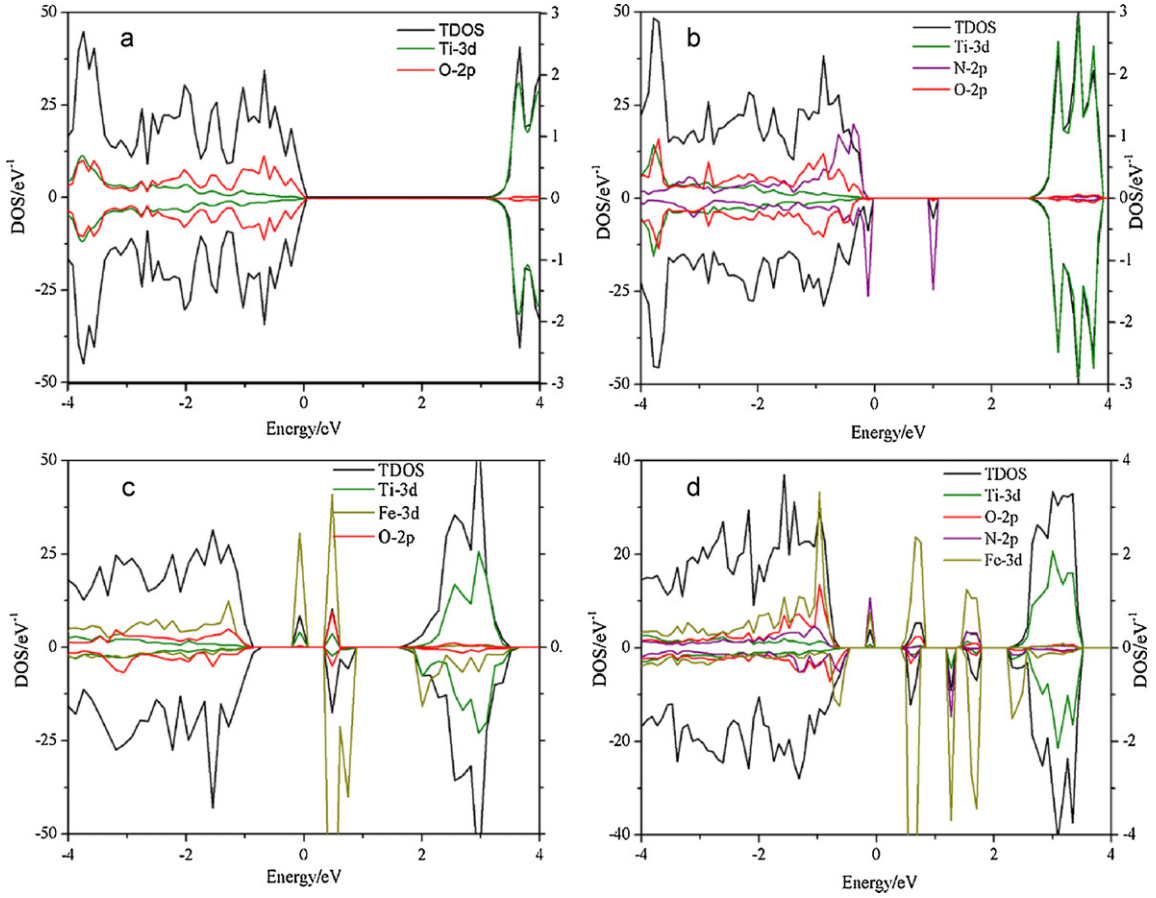

Fig. 3. Calculated DOS and PDOS of: (a) pure TiO_2, (b) N-doped TiO_2, (c) Fe-doped TiO_2, and (d) (N, Fe)-codoped TiO_2. The Fermi level is set to be 0 eV on the energy axis. Curves above and below the horizontal axis refer to the up-spin and down-spin DOS, respectively.

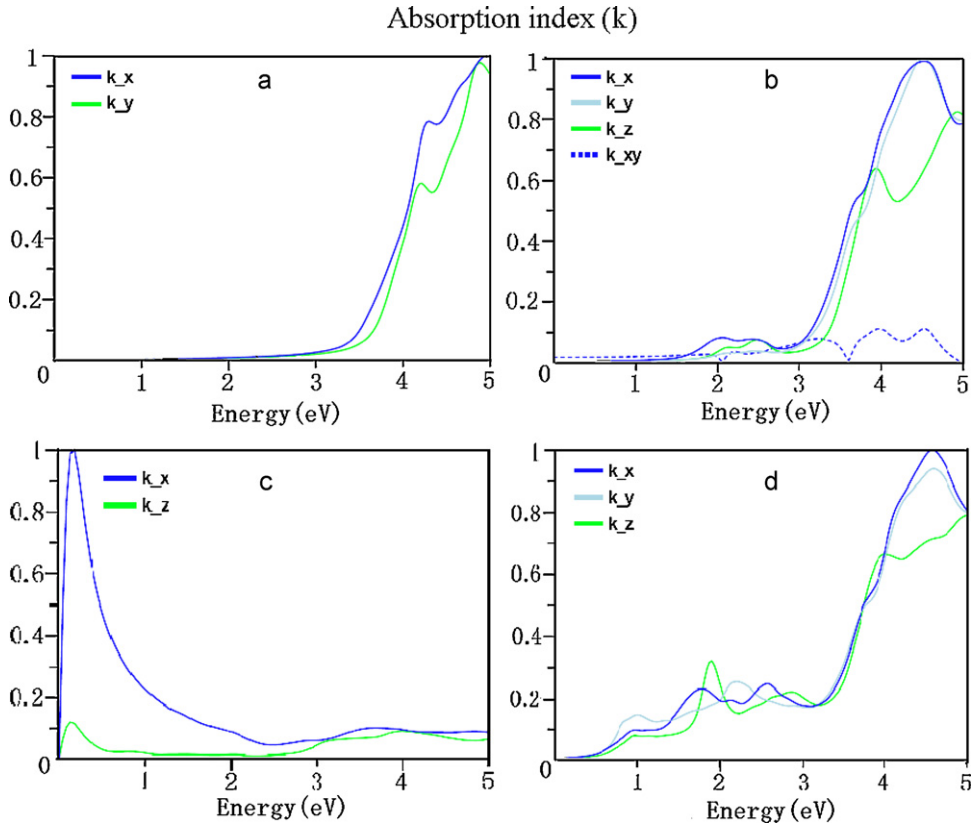

Fig. 4. The optical absorption curves calculated for various types of ion-doped TiO_2: (a) pure TiO_2, (b) N-doped TiO_2, (c) Fe-doped TiO_2, and (d) (N, Fe)-codoped TiO_2.

The absorption edge of the N-doped TiO_2 is shifted to about 1.5 eV, indicating that the photo-excited carrier transition energy is reduced to 1.5 eV, as presented in Fig. 2b. The photo-excited carrier will be trapped by the impure state (N 2p state) and then transferred into the conduction band. The distance between the impure state and the conduction band is 1.5 eV. As shown in Fig. 4c, the Fe-doped system does not show good absorption activity in the visible-light region, whereas a distinct peak appears at about 0.3 eV. Considering Figs. 2c, 3c and 4c together, it can be found that this peak is determined by the band gap near the Fermi level. For the codoped system, the transition energy become smaller due to the split of the impure state, rendering a more obvious red-shift. The efficiency of photocatalytic activity is also promoted by preventing the recombination of electron–hole pairs. Compared with the N-doped and Fe-doped TiO_2, the codoped TiO_2 is expected to be a more active photocatalyst.

4. Conclusions

In this paper, the electronic and the optical properties of N- and/or Fe- doped anatase TiO_2 were calculated and analyzed by means of density functional theory. The results shows that codoping by N and Fe leads to lattice distortion, which in turn changes the dipole moments and makes the separation of the photo-excited electron–hole pairs easier. The impure states appear in the forbidden gap due to the hybridization effect of Fe 3d, N 2p O 2p and Ti 3d states. The absorption spectra show that a significant red-shift occurs upon N and Fe codoping, promoting the efficiency of the photocatalytic activity. The result suggests that the N and Fe codoped TiO_2 is a highly active photocatalyst for efficient visible-light photocatalysis.

Acknowledgments

This research was financially supported by National Science Foundation of China under contract No. 50902056, Scientific Research Foundation for the Returned Overseas Chinese Scholars of Ministry of Education, Fundamental Research Funds for the Central Universities (HUST 2010MS087), and the State Key Lab of Material Processing and Die & Mould Technology.

References

[1] A. Fujishima, K. Honda, Nature 238 (1972) 37–38.
[2] J. Tang, Z. Zou, J. Ye, Catal. Lett. 92 (53) (2004) 53–56.
[3] A.M. Volodin, Catal. Today 58 (103) (2000) 103–114.
[4] U. Diebold, Surf. Sci. Rep. 48 (2003) 53–229.
[5] J.L. Gole, J.D. Stout, C. Burda, Y. Lou, X. Chen, J. Phys. Chem. B 108 (2004) 1230–1240.
[6] R.M. Mohamed, I.A. Mkhalid, J. Alloys Compd. 501 (2010) 143–147.
[7] C. Karunakaran, A. Vijayabalan, G. Manikandan, P. Gomathisankar, Catal. Commun. 12 (2011) 826–829.
[8] Y. Gai, J. Li, S.S. Li, J.B. Xia, S.H. Wei, Phys. Rev. Lett. 102 (2009) 036402.
[9] G. Shao, J. Phys. Chem. C 113 (2009) 6800–6808.
[10] J.S. Wang, Z.Z. Wang, H.Y. Li, Y.T. Cui, Y.C. Du, J. Alloys Compd. 494 (2010) 372–377.
[11] S. Sato, Chem. Phys. Lett. 123 (1986) 126–128.
[12] R. Asahi, T. Morikawa, T. Ohwaki, K. Aoki, Y. Taga, Science 293 (2001) 269–271.
[13] C.D. Valentin, G. Pacchioni, A. Selloni, Phy. Rev. B 70 (2004) 085116.
[14] Q.L. Li, C.R. Zhang, J.Q. Li, J. Alloys Compd. 509 (2011) 1953–1957.
[15] G.Q. Wang, W. Lan, G.J. Han, Y. Wang, Q. Su, X.Q. Liu, J. Alloys Compd. 509 (2011) 4150–4153.
[16] B. Chi, L. Zhao, T. Jin, J. Phys. Chem. C 111 (2007) 6189–6193.
[17] C. Fu, T.Z. Li, J.S. Qi, J. Pan, S.H. Chen, C. Cheng, Chem. Phys. Lett. 494 (2010) 117–122.
[18] X.D. Zhang, M.L. Guo, C.L. Liu, W.X. Li, X.F. Hong, Appl. Phys. Lett. 93 (2008) 012103.
[19] Z. Lin, A. Orlov, R.M. Lambert, M.C. Payne, J. Phys. Chem. B 107 (2003) 5483–5486.
[20] D.W. Jing, Y.J. Zhang, L.J. Guo, Chem. Phys. Lett. 415 (2005) 74–78.
[21] W. Mu, J.M. Herrmann, P. Pichat, Catal. Lett. 3 (1989) 73–84.
[22] Y.L. Su, Y.T. Xiao, Y. Li, Y.X. Du, Y.L. Zhang, Mater. Chem. Phys. 126 (2011) 761–768.
[23] D.E. Gu, B.C. Yang, Y.D. Hu, Catal. Commun. 9 (2008) 1472–1476.
[24] Z.Y. Zhao, Q.J. Liu, Catal. Lett. 124 (2008) 111–117.
[25] M. Pelaez, A. Cruz, S. Stathato, P. Falaras, D. Dionysiou, Catal. Today 144 (2009) 19–25.
[26] R. Long, N.J. English, Chem. Phys. Lett. 478 (2009) 175–179.
[27] R. Long, N.J. English, Chem. Mater. 22 (2010) 1616–1623.
[28] X.X. Yang, C.D. Cao, L. Erickson, K. Hohn, R. Maghirang, K. Klabunde, Appl. Catal. B 91 (2009) 657–662.
[29] K. Iijima, M. Goto, S. Enomoto, H. Kunugita, K. Ema, M. Tsukamoto, N. Ichikawa, H. Sakama, J. Lumin. 128 (2008) 911–913.
[30] G. Kresse, J. Hafner, Phys. Rev. B 49 (1994) 14251–14269.
[31] G. Kresse, J. Furthermuller, Phys. Rev. B 54 (1996) 11169–11186.
[32] J.P. Perdew, K. Burke, M. Ernzerhof, Phys. Rev. Lett. 77 (1996) 3865–3868.
[33] H.J. Monkhorst, J.D. Pack, Phys. Rev. B 13 (1976) 5188–5192.
[34] S.L. Dudarev, G.A. Botton, S.Y. Savarsov, C.J. Humphreys, A.P. Sutton, Phys. Rev. B 57 (1998) 1505–1509.
[35] L. Kavan, M. Gratzel, S.E. Gilbert, C. Klemenz, H.J. Scheel, J. Am. Chem. Soc. 118 (1996) 6716–6723.
[36] J.K. Burdett, T. Hughbandks, G.J. Miller, J.W. Richardson, J.V. Smith, J. Am. Chem. Soc. 10 (1987) 3639–3646.